Impact of gas-phase reactions in the mixing region upstream of a diesel fuel autothermal reformer

Inyong Kang[1], Hans-Heinrich Carstensen, Anthony M. Dean*

Chemical Engineering Department, Colorado School of Mines, 1500 Illinois Street, Golden, CO 80401, USA

ARTICLE INFO

ABSTRACT

The use of diesel fuel to power a solid oxide fuel cell (SOFC) presents several challenges. A major issue is deposit formation in either the external reformer, the anode channel, or within the SOFC anode itself. One potential cause of deposit formation under autothermal reforming conditions is the onset of gas-phase reactions upsteam of the catalyst to form ethylene, a deposit precursor. Another potential problem is improper mixing of the fuel, air, and steam streams. Incomplete mixing leads to fuel rich gas pockets in which gas phase pyrolysis chemistry might be accelerated to produce even more ethylene. We performed a combined experiment/modeling analysis to identify combinations of temperature and reaction time that might lead to deposit formation. Two alkanes, n-hexane and n-dodecane, were selected as surrogates for diesel fuel since a detailed mechanism is available for these species. This mechanism was first validated against n-hexane pyrolysis data. It was then used to predict fuel conversion and ethylene production under a variety of reforming conditions, ranging from steam reforming to catalytic partial oxidation. Assuming that the reactants are perfectly mixed at 800 K, the predictions suggest that a mixture must reach the catalyst in less than 0.1 s to avoid formation of potentially troublesome quantities of ethylene. Additional calculations using a simple model to account for improper mixing demonstrate the need for the components to be transported to the catalyst on a much shorter time scale, since both the relatively lean and relatively rich regions react faster and rapidly form ethylene.

1. Introduction

The use of solid-oxide fuel cells as auxiliary power units (APUs) on long-haul trucks could provide the necessary power to allow the diesel engine to be shut down during rest intervals while the APU, running on diesel fuel, would provide the required power for the driver's compartment. Such an approach has several advantages, including improved efficiency, quiet operation, and a reduction of emissions. A key component of such a system is the catalytic reformer which converts the liquid diesel fuel into synthesis gas for SOFC operation. However, reforming of diesel fuel has presented problems in the past [1]. The research group of Bae has studied autothermal reforming (ATR) of diesel fuels and concluded that gas phase reactions in the mixing zone upstream of the reformer lead to the formation of deposit precursors which subsequently deactivate the reforming catalyst [2–5]. If the catalyst is deactivated, hydrocarbons are not longer completely reformed, and some will reach the anode of the SOFC. In the high-temperature reducing environment

of the anode, these hydrocarbons are prone to form deposits that can not only restrict the passage of gas to the three-phase region but also deactivate the anode catalyst, resulting in lower SOFC power and perhaps even cell failure.

Some representative experimental evidence that led to this conclusion is shown in Fig. 1. The top panel shows the results of an experiment in which a surrogate diesel fuel, steam and air were mixed and then introduced into a heated reformer (1073 K). The exit products were identified and quantified via GC. Results are shown for two cases: the first experiment used a blank reactor while the second one was performed with a catalyst loaded reactor. As expected, the presence of a reforming catalyst led to 100% conversion, producing mostly synthesis gas, with small amounts of methane and ethylene being also produced. Notably, the blank reactor also converted ~50% of the diesel fuel, indicating the importance of gas-phase chemistry under these conditions. The gas-phase reactions produced significant amounts of ethylene and propylene, species that are likely to participate in reactions that lead to molecular weight growth. Another important observation is the high yield of CO_2. This can be rationalized by assuming that part of the fuel was completely oxidized instead of being only partially oxidized to CO. The production of significant amounts of ethylene as well as high CO_2 yields suggests that zones of fuel rich and lean fuel mixtures are formed next to each other due to incomplete
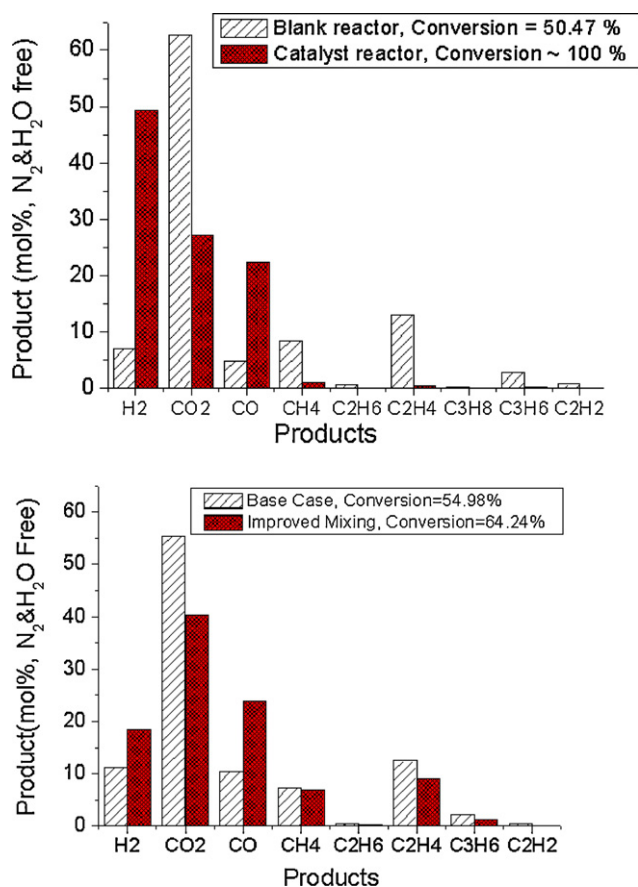

Fig. 1. Observed exit product distributions, excluding H_2O, with a surrogate diesel fuel passing through an ATR reactor (O/C = 1.4, 1073 K, τ = ~1.5 s). (Top) Comparison of the products with and without catalyst (S/C = 1.25) [3]; (bottom) effect of improved mixing (S/C = 3) for a case with no catalyst [4].

mixing. A (relatively) fuel-rich region would lead to pyrolysis products such as the olefins, while a (relatively) fuel-lean environment would promote the CO_2 formation. The results presented in the lower panel of Fig. 1 are consistent with this hypothesis. Here the use of an improved mixer led to increased synthesis gas production with lower yields of CO_2 and C_2 and C_3 species.

The present study builds on this interpretation and aims to provide a more detailed analysis of the potential for gas-phase reactions within the mixing region to play a role. It is desirable to minimize such reactions, since these are typically not as selective as the catalytic reactions. In particular, it is critical to avoid production of olefins such as ethylene that are deposit precursors. Olefin production would increase the potential for catalyst deactivation within the reformer. This in turn could lead to slippage of olefins through the reformer, allowing them to form deposits within the SOFC. We investigate the impact of different reformer operating modes (varied O/C and S/C), different fuels (n-hexane and n-dodecane), and temperature on the time scale required for gas-phase chemistry to begin. This information helps to set an upper limit on the amount of time that can be spent in the mixing region. We also begin to explore the impact of imperfect mixing upstream of the reformer. The kinetic models used for this analysis are validated against experimental observations of hexane pyrolysis.

2. Experiment and model descriptions

A diagram of the experimental setup is shown in Fig. 2. Briefly, a gas mixture consisting of a hydrocarbon diluted with an inert gas

is sent through a heated tubular reactor and the final products of the effluent are analyzed gas chromatographically.

n-Hexane (nC_6H_{14}) was selected as a surrogate for diesel fuel. It was purchased from Sigma–Aldrich (~97% HPLC grade). A GC analysis of the n-hexane fuel revealed that the ~3% impurities consisted of other C_6 isomers. Liquid n-hexane was supplied to a heated metal vaporizer via a milliGAT pump. OMEGALUX heat tape (423–473 K) was used to maintain the temperature of the vaporizer above the boiling point of n-hexane. The vaporized fuel then flowed into a mixing chamber where N_2 gas was added. All lines following the vaporizer were heated between 393 and 473 K to avoid condensation of larger alkanes (e.g., C_6 and larger).

A quartz tube of 0.6 cm inner diameter was used as the reactor. It was housed in a furnace equipped with three dedicated Eurotherm 2216e PID temperature controllers. The length of the heated zone was 32 cm. The temperature profile within the heated zone along the centerline of the reactor was experimentally determined with a thermocouple. Temperatures were measures in 1 cm intervals. The profiles revealed that the temperature in the center of the furnace/reactor was very constant and it changed sharply only at the beginning and the end of the reactor.

A Hewlett-Packard 5890 Series II+ gas chromatograph was used to measure the mole fraction of all hydrocarbon species from C_1 to C_{11}. The species were separated on a Supelco SPB-1 (60 m × 0.53 mm ID, 5 μm fused silica film column) that was connected to a FID. The GC was calibrated for the gases of interest and yielded quantitative concentration measurements with a relative error of ~3%. In addition, the reactor effluent was sent to a mass spectrometer (MKS Cirrus LM 99) that provided a semi-quantitative analysis of the species composition and was also used to verify that steady-state conditions were reached prior to collecting data.

The n-hexane experiments were performed over a wide range of temperatures (823–1048 K) at two residence times (~1 s and ~5 s). The nominal mole fractions of n-hexane/N_2 used are 0.1/0.9 for the experiments at ~1 s and 0.5/0.5 for the ~5 s experiments. The initial flow rates were held constant as the temperatures were varied, leading to small variations in the actual residence times. The measured reactor pressure was ~0.8 atm.

The modeling predictions used two mechanisms. The CSM kinetic mechanism was used to describe hexane pyrolysis; it consists of 1616 reactions and 216 species. It has been described by Randolph and Dean [6]. The current version contains a few modifications introduced by Al Shoaibi [7] to improve predicted conversions and product selectivities for a series of alkane and alkene pyrolysis reactions. These modifications consist of modest changes of six rate constants; five of the changes involve the initiation reactions for ethane, isobutane, and n-hexane, and the sixth is the dissociation of ethyl to ethylene and H radical. A Lawrence Livermore National Laboratories (LLNL) mechanism was used for both n-hexane and n-dodecane [8]. The LLNL model consists of 2115 species and 8157 reactions and was developed to describe pyrolysis and oxidation of large alkanes. It includes both high- and low-temperature pathways and was validated against an extensive database. The calculations were done with the plug-flow reactor model of the CHEMKIN software [9]. Measured temperature–distance profiles were used as input to the models when comparing the predictions to the observed n-hexane pyrolysis results.

3. Results and discussion

3.1. N-hexane pyrolysis experiments and modeling predictions

Vaporized n-hexane fuel diluted with N_2 is passed through the heated quartz reactor. The effluent is directly sent into both the GC
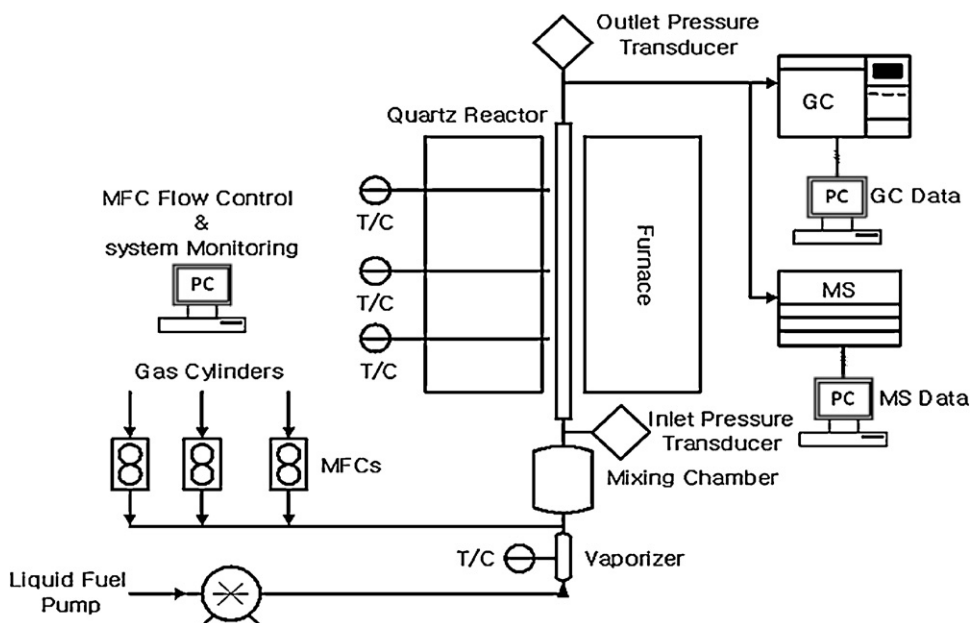
Fig. 2. Schematic diagram of the flow reactor system.

and MS to monitor overall consumption of n-hexane as well as the product distribution. The observed n-hexane conversion, shown in Fig. 3, varies from ~1% to ~98% (T = 825–1050 K, τ ~1 s) and from ~10% to ~87% (T = 825–950 K, τ ~5 s). Both the unadjusted CSM and LLNL kinetic models capture the effect of temperature as well as residence time on the fuel conversion. Similarly, both mechanisms properly predict the effect of temperature of the major product distributions at τ ~1 s (Fig. 4). Note that ethylene is the major product of n-hexane pyrolysis. Higher olefins such as propylene and butadiene are also produced. The observed decreases in the C_3, C_4, and C_5 species concentrations at the higher temperatures correspond to the onset of production of heavier species (Fig. 5). The mass spectrometer fragmentation pattern for the major C_7 species suggests that it is toluene. When the experiments were completed, substantial amounts of deposits were observed within the quartz reactor. These observations document the potential for substantial deposit formation if alkanes such as hexane are allowed to remain in a pyrolyzing environment for times on the order of 1 s or longer if the temperature reaches or exceeds 700 °C.
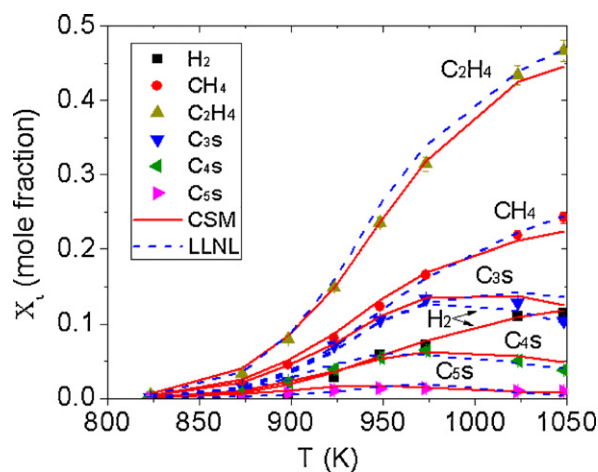

Fig. 4. Comparison of observed and predicted major product distributions in n-hexane pyrolysis (n-C_6H_{14}/N_2 = 0.1/0.9, τ = ~1 s, P = 0.8 atm, N_2 free basis).
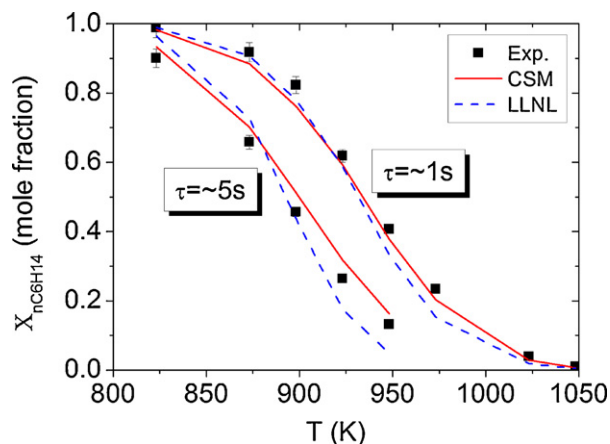
Fig. 3. Comparison of observed and predicted n-hexane conversions (n-C_6H_{14}/N_2 = 0.1/0.9 for τ = ~1 s and 0.5/0.5 for τ = ~5 s, P = 0.8 atm). Results are plotted on a N_2 free basis.
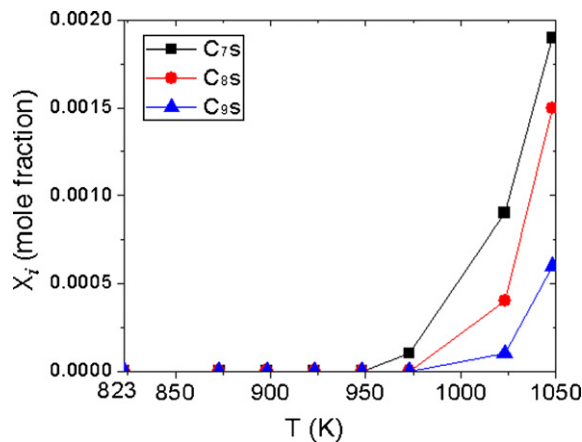
Fig. 5. Observed production of higher hydrocarbons (C_7s, C_8s, C_9s) during n-hexane pyrolysis (n-C_6H_{14}/N_2 = 0.1/0.9, τ = ~1 s, P = 0.8 atm, N_2 free basis).

Table 1
Summary of initial conditions.

	O/C	S/C	n-C6H14 case (mole fraction)				n-C12H26 case (mole fraction)			
			nC6	O2	N2	H2O	nC12	O2	N2	H2O
L-ATR	0.36	1.25	0.073	0.079	0.298	0.550	0.038	0.082	0.309	0.571
ATR[a]	0.72	1.25	0.053	0.115	0.432	0.399	0.027	0.118	0.444	0.410
CPOX	1	0	0.065	0.196	0.738	–	0.034	0.203	0.763	–
H-ATR	1.4	1.25	0.035	0.147	0.554	0.263	0.018	0.150	0.564	0.268
SR	0	2	0.071	–	0.071	0.857	0.039	–	0.039	0.923

[a] Thermoneutral condition ($\Delta H_r \approx 0$).

The good agreement between the two models and the observed n-hexane pyrolysis data is encouraging. Since the LLNL model was primarily developed to describe the oxidation reactions of higher hydrocarbons, it ability to also predict n-hexane pyrolysis suggests that it is a suitable tool to explore the reactions of such hydrocarbons at the fuel/steam/air conditions encountered in ATR. In this context, the predicted rate of ethylene production in the mixing region is expected to correlate with the propensity to form deposits on the reformer catalyst.

3.2. Model predictions for n-hexane and n-dodecane reactions in the mixing region

To investigate the impact of various reforming conditions on the potential for gas-phase reactions in the mixing region, five representative conditions were considered: endothermic ATR ('L-ATR'), thermoneutral ATR ('ATR'), exothermic ATR ('H-ATR'), catalytic partial oxidation ('CPOX') and steam reforming ('SR'). Table 1 shows the initial conditions used. Note that the mole fraction of dodecane is approximately one-half that of hexane to reflect the larger number of carbon atoms in dodecane.

Fig. 6 illustrates the predicted effect of temperature and residence time on the reaction of n-hexane for the thermoneutral (ATR) case. Essentially, no reaction occurs below 760 K. With increasing temperature, the conversion of n-hexane rapidly increases, as shown in the top panel of Fig. 6. This conversion is associated with the production of substantial amounts of ethylene, as shown in the bottom panel of the figure. Note that ethylene is formed prior to the increase in temperature, suggesting that the production of deposit precursors precede the exothermic oxidation reactions. The increase in temperature indicates the onset of oxidation; at this point a small fraction of the ethylene is consumed. Even though this is theoretically a thermoneutral case (i.e., if this system were to react to reach complete equilibrium, the temperature would return to the initial temperature), note the large (300–400 K) rise in temperature during the oxidation stage. The system is still far from equilibrium; at much longer reaction times temperature will decrease as the slower (especially in the gas-phase) endothermic
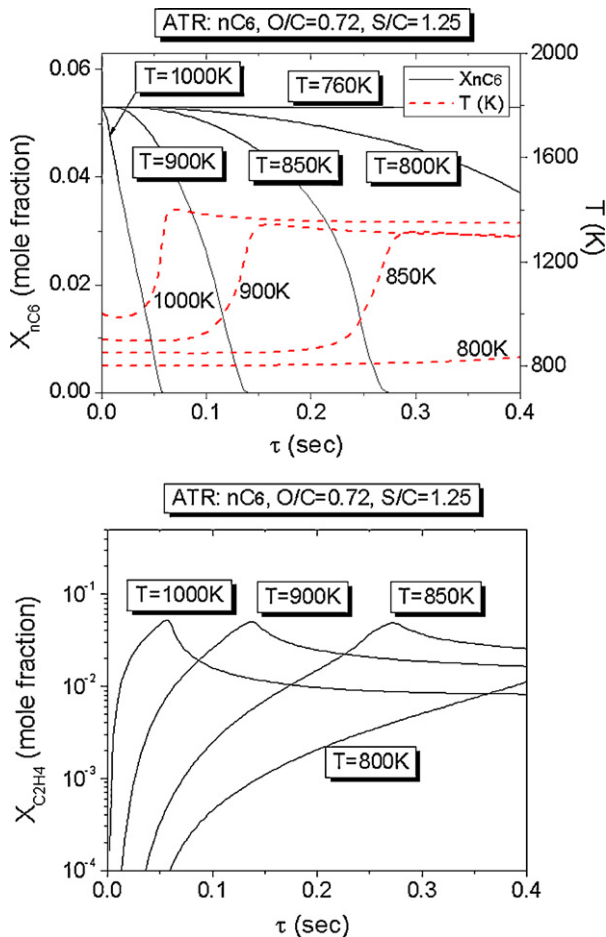

Fig. 6. Predicted effect of inlet temperature on n-hexane conversion, reaction temperature and ethylene production for the ATR case (cf. Table 1).
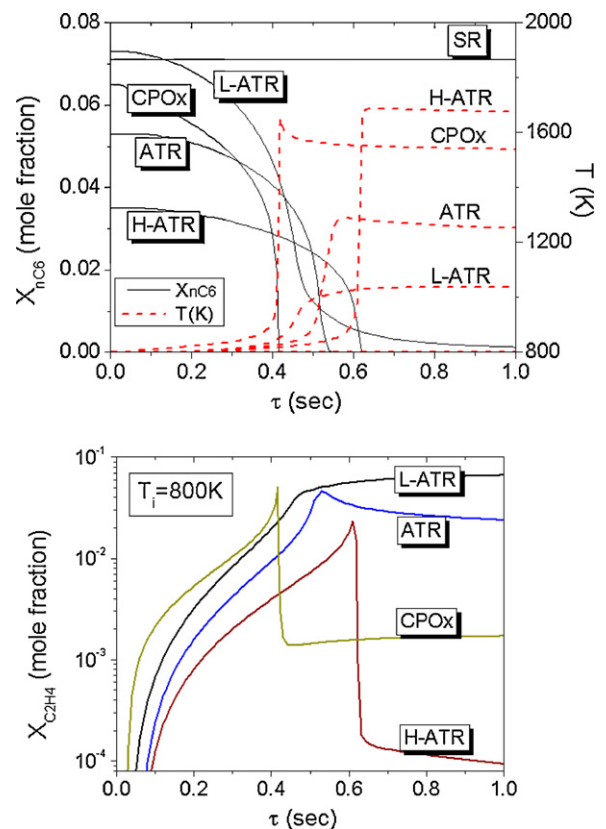

Fig. 7. Predicted impact of varying O/C and S/C ratios on gas-phase reactivity. Cf. Table 1 for mixture compositions.
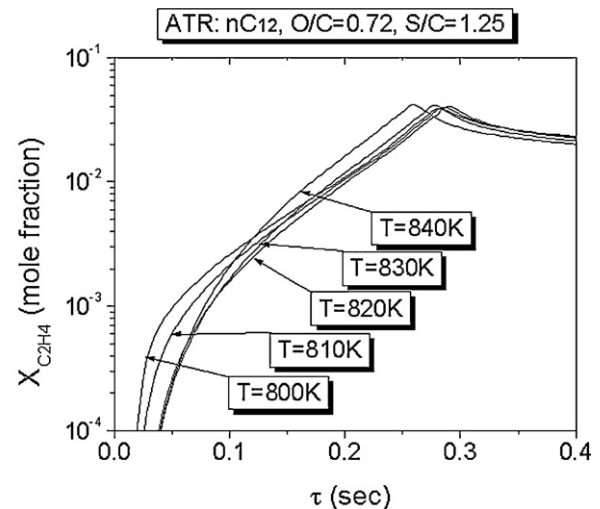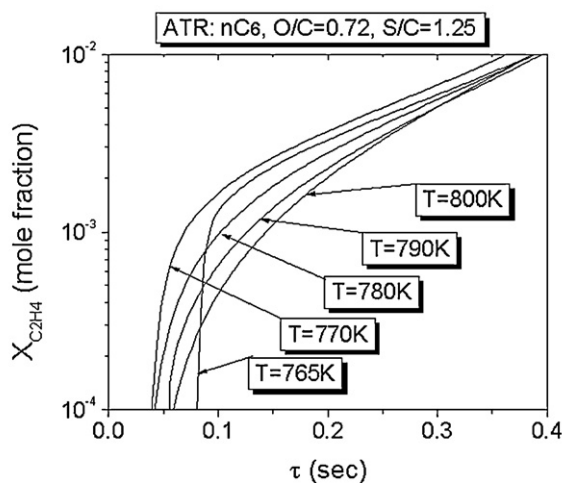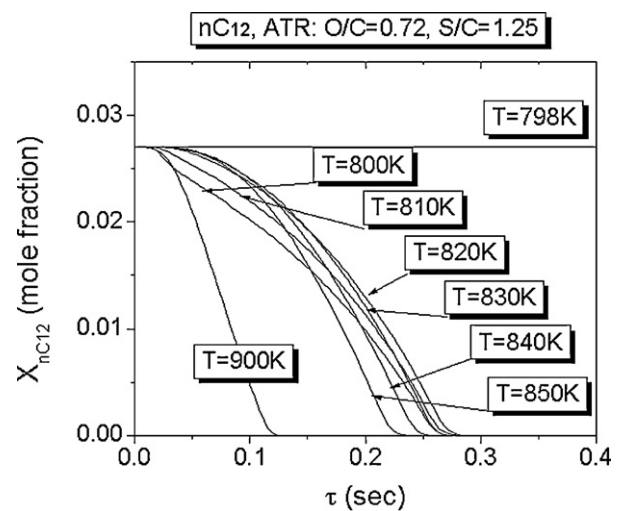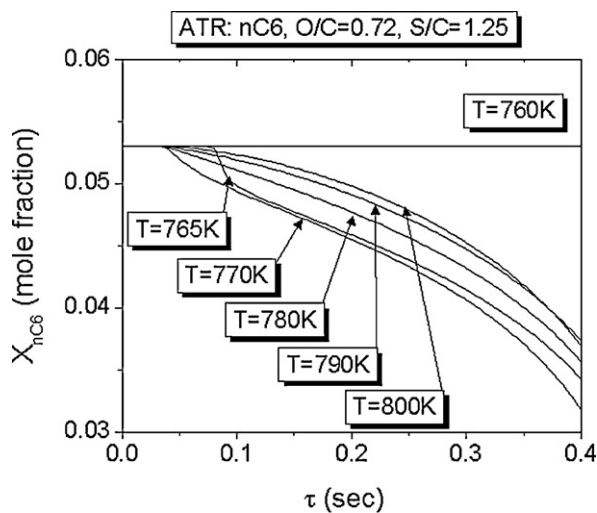
Fig. 8. Predicted impact of initial temperature on reactivity of n-hexane for the ATR case (cf. Table 1).

Fig. 9. Predicted impact of initial temperature on the reactivity of n-dodecane for the ATR case (cf. Table 1).

steam reforming reactions occur. These calculations suggest the potential for significant reformer operational problems if the temperature in the mixing region is ~800 K or above unless the mixing times are very short. One issue is the formation of deposits as the ethylene formed leads to molecular weight growth reactions. Another problem is that the large increase in temperature, e.g., ~450 K for the 850 K case, due to the gas-phase oxidation might be sufficient to sinter the catalyst.

Fig. 7 shows the predicted impact of varying O/C and S/C (with hexane as the fuel) at a fixed initial temperature of 800 K. With the exception of steam reforming, reaction begins, accompanied by rapid ethylene production, within ~0.1 s. Very large temperature excursions are predicted at longer times (0.4–0.6 s). Even the L-ATR case (the "endothermic" case) exhibits a temperature rise of over 200 K. The more oxidizing cases (CPOX and H-ATR) exhibit sharp drops in ethylene concentrations as the oxidation process begins, but these cases also induce the largest temperature excursions. The variation in reactivity for the various mixtures reflects the complexity of the kinetics. The different initial conditions lead to different reaction rates; also the different heat capacities of the various mixtures affect the magnitude of the temperature rise. Among the autothermal reforming cases, the L-ATR case (with the lowest O/C) is predicted to be the fastest while the H-ATR case, with the highest O/C, is the slowest. Note that significant amounts of n-hexane are reacted prior to the temperature increase. This is a manifestation of pyrolysis kinetics, and the rates correlate with the

initial fuel mole fraction. The CPOX has the highest O/C ratio, and it is the fastest; the lower heat capacity for this case leads to a more rapid temperature rise. The results suggest that, if the reactants are to be mixed at a temperature as high as 800 K, a mixer design must be chosen that permits complete mixing (and delivery of the mixture to the catalyst) in well less than 100 ms to avoid formation of potentially troublesome quantities of ethylene that can lead to deposit formation on the catalyst.

The impact of lower temperatures on the reactivity of the ATR hexane mixture is shown in Fig. 8. Note the rapid onset of reactivity just above 760 K, as shown in the top panel. Interestingly we see an unusual effect of temperature between 765 and 800 K; the rate first increases and then slows down again between 770 and 800 K. This behavior is indicative of the Negative Temperature Coefficient (NTC) behavior often observed in the ignition of hydrocarbons fuels [8]. The bottom panel shows a very rapid increase in ethylene production in less than 100 ms. The predictions suggest that the mixing of steam, air, and fuel should be complete and that the mixture would need to enter the catalyst bed within ~50 ms if the components enter the mixing region at a temperature of 500 °C. Although not shown in this figure, predictions for the other autothermal reforming cases exhibit similar behavior.

The predictions for the effect of temperature on the thermoneutral mixture (ATR) containing n-dodecane are shown in Fig. 9. The results are quite similar to those for n-hexane. This system

Table 2
Summary of predicted results for various reforming options at conditions at which gas-phase reactions can become important.

	n-C$_6$H$_{14}$			n-C$_{12}$H$_{26}$		
	T (K)[a]	$t_{5\%}$ (s)[b]	t_t (s)[c]	T (K)[a]	$t_{5\%}$ (s)[b]	t_t (s)[c]
L-ATR	755	0.072	0.068	790	0.028	0.044
ATR	765	0.088	0.096	800	0.028	0.052
H-ATR	770	0.08	0.092	805	0.068	0.112
CPOX	795	0.112	0.1	815	0.024	0.032
SR	900	0.66	0.015	880	0.79	0.19

[a] Threshold temperature for reaction to occur.
[b] Residence time for 5% fuel conversion.
[c] Threshold residence time for C$_2$H$_4$ mole fraction to reach 0.001.

is predicted to be slightly less reactive, with the temperatures for a comparable level of reaction shifted upwards by ~40 K. Here fuel conversion begins at around 800 K. However, note that the predicted time for onset of ethylene production at this temperature is approximately half the time predicted for n-hexane (cf. Fig. 8) at its conversion onset temperature. One reason for the increased ethylene production rate is simply that there are twice as many –CH$_2$CH$_2$– units in n-dodecane that can from ethylene during pyrolysis.

The results of all the predictions for both n-hexane and n-dodecane are summarized in Table 2. Three parameters are listed for each calculation: (1) The temperature at which reaction first begins. (2) The time required for 5% of the fuel to be consumed. (3) The time required for the ethylene mole fraction to reach 0.001. This ethylene mole fraction level was selected since this is the level at which it has been observed to begin to form deposits [5]. Not surprisingly, the least reactive system is steam reforming (SR) and so even quite long mixing times are unlikely to result in any significant gas-phase chemistry for this case. Not only is steam unreactive below 900 K, but also the steam dilutes the fuel, thereby slowing down the pyrolysis kinetics. Once air is added, the system is much more reactive, and the time available to achieve complete mixing is generally on the order of 100 ms or even less. Interestingly, once
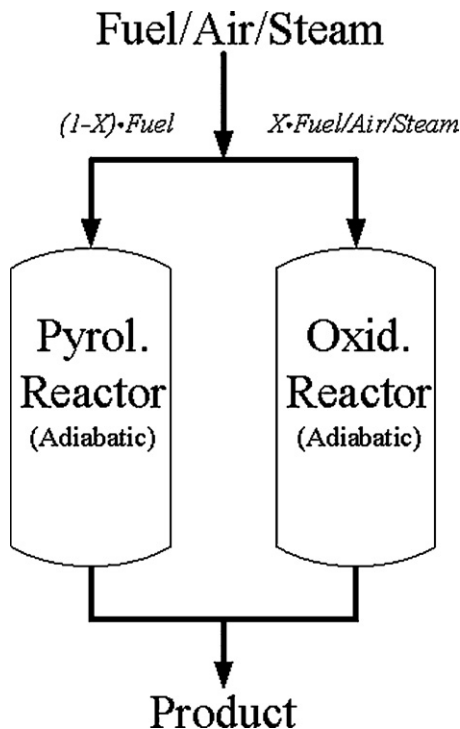

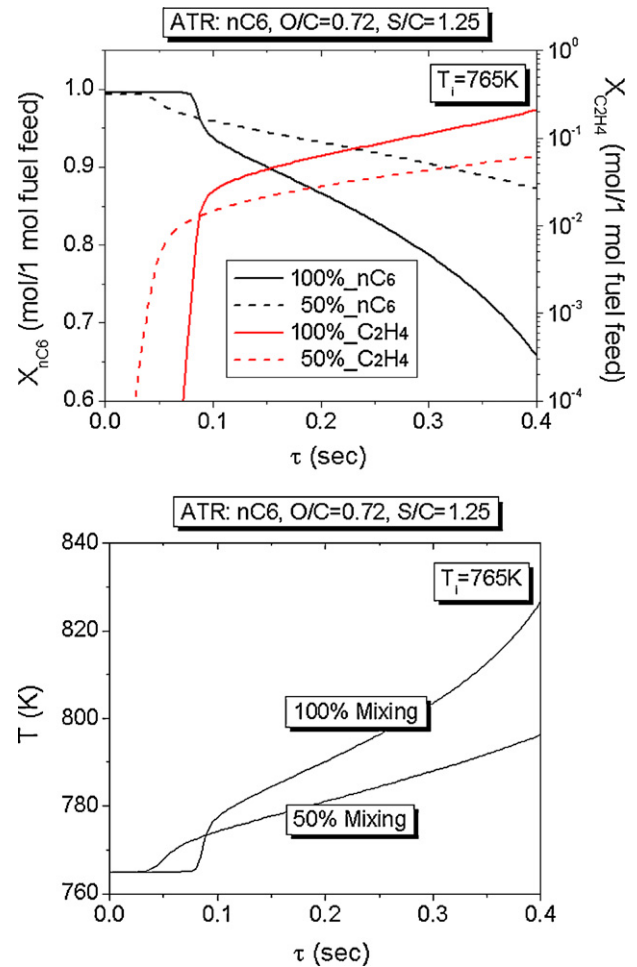**Fig. 10.** Reactor model used to simulate imperfect mixing.

Fig. 11. (Top) Comparison of n-hexane conversion and ethylene production for the perfectly mixed ATR case to that predicted when half of the n-decane is pyrolyzed while the other half mixed perfectly with all of the steam and air. (Bottom) Predicted temperature profiles.

air is present, the results are quite similar regardless of the amount of air added, even up to CPOX conditions where there is no steam to act as a diluent.

3.3. Impact of imperfect mixing

The results discussed so far assumed homogenous initial gas compositions. However, complete mixing is a difficult task to achieve—especially on short time scales. To assess the impact of incomplete mixing on the gas-phase reactions upstream of a diesel ATR catalyst bed, we used the LLNL kinetic model in conjunction with the reactor system shown in Fig. 10. Two adiabatic reactors are arranged in parallel and the fuel/steam/air feed is divided such that a fraction of the fuel (with no steam or air) is fed to one reactor (Pyrolysis) while the remaining fuel (with all of the steam and air) is sent to the second reactor (Oxidation). In the Oxidation reactor it was assumed that fuel, air and steam are perfectly mixed. The product streams from each reactor are then combined to represent the final product. Clearly this model is a vast oversimplification of reality, but it allows one to begin to explore the situation where, for example, a portion of the fuel remains unmixed, resulting in pyrolysis chemistry, while the remaining fuel reacts in an environment that is more oxidizing than if the entire system were well-mixed.

The predictions for the n-hexane ATR case, assuming 50% mixing (i.e., where half the fuel is fed to the Pyrolysis reactor and the remaining half is fed with all of the air and steam to the Oxida-
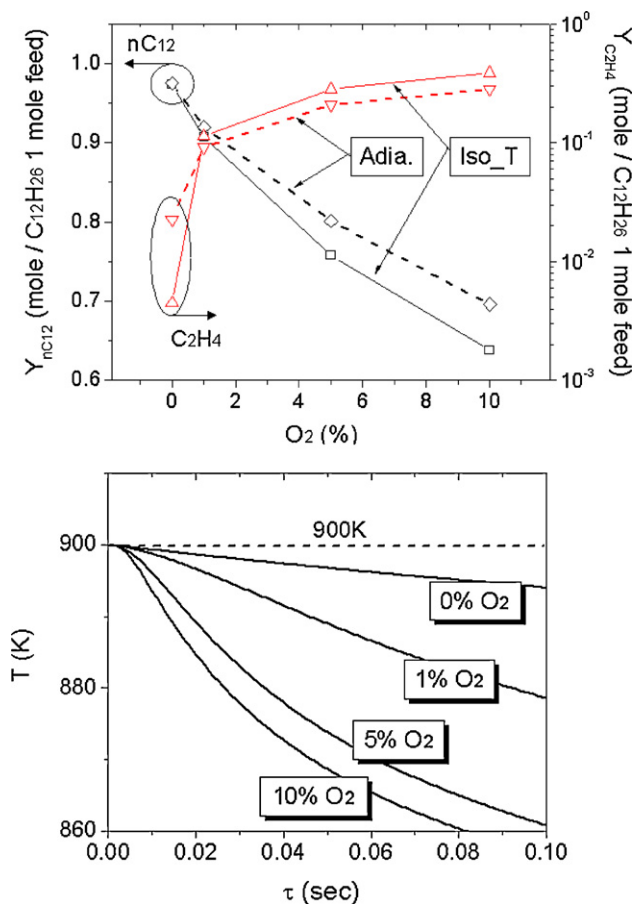
Fig. 12. Predicted impact of the addition of small amounts of O_2 to n-dodecane ($T = 900$ K, $t = 0.1$ s). (Top) Effect on conversion and ethylene production. (Bottom) Effect of O_2 addition on the temperature–time profile.

tion reactor) are compared to the perfectly mixed results in Fig. 11. The upper panel shows that the partially mixed case leads to much faster reaction, with now all of the reaction occurring in the Oxidation reactor. In this reactor the O/C ratio is twice that of the perfectly mixed case and the partial oxidation reactions are accelerated. Note that the temperature rise in this reactor occurs at the same time at which a significant amount of ethylene is produced. In contrast, there is no reaction in the Pyrolysis reactor. For the well-mixed case 765 K is the lowest temperature at which reaction occurs. The lack of any oxygen in the Pyrolysis reactor slows down the ignition kinetics such that a higher temperature is required for reaction to begin.

Another approach to begin to assess the impact of imperfect mixing is to explore the impact of adding small amounts of oxygen to the Pyrolysis reactor. A series of cases were run in which increasing amounts of O_2 were added to n-dodecane. (Even at the highest level of added O_2 (10%), the system is still very fuel-rich.) The results are shown in Fig. 12. At an initial temperature of 900 K, only ~2% of the fuel is converted at 0.1 s residence with no added O_2. Addition of O_2 significantly increases both n-dodecane conversion and ethylene production (Note the log scale for ethylene.). The impact is not quite so large under adiabatic conditions since the oxygen-enhanced pyrolysis leads to a drop in temperature, slowing down the reaction.

These predictions illustrate some of the operational difficulties that might result for imperfect mixing. Within the mixing region itself, either too little or too much oxygen can lead to enhanced production of ethylene, which in turn increases the likelihood of deposit formation on the catalyst. Another problem is that any (relatively) oxygen-rich packets that reach the catalyst can lead to temperature overshoots within the catalyst bed that could lead to sintering. Of course, the extremely simple mixing models only serve to suggest that mixing is a critical issue. The results are sufficiently worrisome to warrant a detailed investigation in which the reaction kinetics is coupled to a CFD analysis. Such efforts are now underway in our group.

4. Conclusions

The modeling predictions suggest that careful attention should be paid to the design of the mixer upstream of an autothermal reformer. Assuming that the streams can be mixed on the order of 50 ms or less, gas-phase reactions are likely to be unimportant as long as the temperature in the mixing zone is less than 800 K (527 °C). However, if the design is to feed fully vaporized diesel fuel to the mixing region, the temperature of this stream will likely be ~400 °C (This temperature estimate is based on the diesel fuel specification that the maximum temperature at which the 90% fraction of the fuel will distill is 338 °C.). If the steam is to come from anode recycle, ideally that stream should be close to the SOFC exit temperature (~700–800 °C) to avoid efficiency losses. As a consequence, it is certainly possible that the gases in the mixing region can be in a temperature range where the undesired formation of deposit precursors can occur. The predictions also suggest that the situation is even worse if the mixing time is longer. A prudent approach would be to couple a CFD analysis of the proposed mixer design with a detailed kinetic model for the fuel of interest to assess the potential for deposit formation or temperature overshoot.

References

[1] T.R. Krause, S. Ahmed, R. Kumar, The 4th International Conference on Fuel Cell Science, Engineering and Technology, in: Proceedings of Fuel Cell, 2006, FUELCELL2006-97260.
[2] I. Kang, J. Bae, S. Yoon, Y. Yoo, J. Power Sources 172 (2007) 845–852.
[3] S. Yoon, I. Kang, J. Bae, Int. J. Hydrogen Energy 33 (2008) 4780–4788.
[4] S. Yoon, I. Kang, J. Bae, Int. J. Hydrogen Energy 34 (2009) 1844–1851.
[5] I. Kang, S. Yoon, G. Bae, J. Kim, J. Bae, D. Lee, Y. Song, Catal. Today 136 (2008) 249–257.
[6] K.L. Randolph, A.M. Dean, Phys. Chem. Chem. Phys. 9 (2007) 4245–4258.
[7] A. Al Shoaibi, Experimental and Modeling Analysis of Hydrocarbon Pyrolysis. Ph.D. Thesis, Chemical Engineering Department, Colorado School of Mines, Golden, CO, 2008.
[8] C.K. Westbrook, W.J. Pitz, O. Herbinet, H.J. Curran, E.J. Silke, Comb. Flame 156 (2009) 181–199.
[9] ChemKin-Pro, Reaction Design: San Diego, 2008.